Acta Cryst C STRUCTURAL CHEMISTRY

ISSN 2053-2296

Synthesis, structural analysis, and docking studies with SARS-CoV-2 of a trinuclear zinc complex with *N*-phenylanthranilic acid ligands

Armel L. Mbani O.,[a] Evan F. Bonnand,[b] Awawou G. Paboudam,[a] Jacob P. Brannon,[b] Kevyn D. Gardner-Ricossa,[b] S. Chantal E. Stieber[b]* and Moise O. Agwara[a]

[a]Faculty of Science, Department of Inorganic Chemistry, University of Yaoundé I, PO Box 812, Yaoundé, Cameroon, and [b]Department of Chemistry & Biochemistry, California State Polytechnic University, Pomona, 3801 W. Temple Ave., Pomona, CA 91768, USA. *Correspondence e-mail: sestieber@cpp.edu

Received 15 November 2021
Accepted 1 March 2022

Edited by L. Dawe, Wilfrid Laurier University, Waterloo, Ontario, Canada

Keywords: trinuclear; phenylanthranilic acid; NPA; zinc; inorganic chemistry; organometallic; SARS-CoV-2; molecular docking; crystal structure.

CCDC reference: 2155769

Supporting information: this article has supporting information at journals.iucr.org/c

The structure of a trinuclear zinc complex, hexakis(μ_2-2-anilinobenzoato)diaquatrizinc(II), $[Zn_2(C_{13}H_{10}NO_2)_6(H_2O)_2]$ or $(NPA)_6Zn_3(H_2O)_2$ (NPA is 2-anilinobenzoate or *N*-phenylanthranilate), is reported. The complex crystallizes in the triclinic space group $P\overline{1}$ and the central Zn^{II} atom is located on an inversion center. The NPA ligand is found to coordinate *via* the carboxylate O atoms with unique C—O bond lengths that support an unequal distribution of resonance over the carboxylate fragment. The axial H_2O ligands form hydrogen bonds with neighboring molecules that stabilize the supramolecular system in rigid straight chains, with an angle of 180° along the *c* axis. π stacking is the primary stabilization along the *a* and *b* axes, resulting in a highly ordered supramolecular structure. Docking studies show that this unique supramolecular structure of a trinuclear zinc complex has potential for binding to the main protease (M^{pro}) in SARS-CoV-2 in a different location from Remdesivir, but with a similar binding strength.

1. Introduction

The design of zinc complexes as antiviral agents from simple, relatively cheap, and available ligands is of great interest in supramolecular chemistry and materials science (Batten *et al.*, 2009). Coronaviruses such as SARS-CoV can be targeted by Zn^{2+} when combined with ionophores to increase Zn^{2+} concentrations inside the cell (te Velthuis *et al.*, 2010). Zn^{2+} has been proposed for use as a supplement in reducing COVID-19 morbidity (Derwand & Scholz, 2020), with possible impacts on virus replication, neurological damage, and inflammation (Cereda *et al.*, 2022). Current proposed modes of action are through inhibition of DNA and RNA replication (te Velthuis *et al.*, 2010), so the main protease of SARS-CoV-2 (M^{pro}) is of particular interest for developing antiviral agents. M^{pro} plays a key role in the replication and transcription of SARS-CoV-2 and is the target of Remdesivir, the first therapeutic approved by the FDA for COVID-19 treatment (Beigel *et al.*, 2020). Molecular docking studies of Remdesivir with M^{pro}, as compared to other potential antiviral agents, established that Remdesivir binds most strongly to M^{pro} based on the most favorable docking score (Naik *et al.*, 2020). This establishes molecular docking as a possible tool for screening potential antiviral agents. The current work presents the synthesis of a novel trinuclear zinc complex and analysis of its molecular docking to M^{pro}.

Polynuclear complexes can be synthesized using ligands with multidentate moieties (El-Boraey & El-Salamony, 2019),

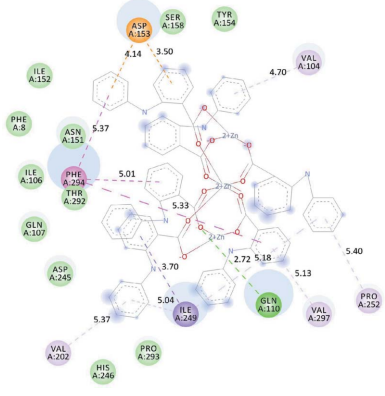

and amino acid-based ligands are often targeted because of their potential pharmacological properties (Aiyelabola *et al.*, 2016). Although the naturally occurring α-amino acids have been studied extensively, synthetic β-amino acids have only more recently been considered for applications in coordination chemistry. This work focuses on *N*-phenylanthranilic acid (NPA), which is a β-amino acid. In β-amino acids, the amino group is bound to the β-carbon, which is one atom further removed from the carboxylic acid group. This contrasts with α-amino acids, in which the carbonyl C atom of the carboxylic acid group and the N atom of the amino group are bound to the same C atom, the α-carbon. Of note are the two arene arms in NPA, which can rotate freely around the amino group. This capacity for rotation minimizes steric hindrance and can therefore lead to interesting structures with versatile motifs.

NPA is reported to act as a chelating ligand for metals, with potential for coordination through both the N atom of the amino group (N) and the O atoms of the carboxyl group ($-COO^-$) (Ros *et al.*, 2002). NPA can also bind either through one carboxylate O atom, as in the motif $Zn(Hdmpz)_2(L_2)_2$ (Hdmpz is 3,5-dimethylpyrazole and L_2 is *N*-phenylanthranilate), or through both carboxylate O atoms, as in the dinuclear motif $[Cu_2(C_6H_5NHC_6H_4COO)_4(CH_3CH_2OH)_2]$ (Jin & Wang, 2014; Taş *et al.*, 2010). NPA ligands were reported to coordinate to rhodium for synthesizing hydrogenation catalysts, as seen in RhPAA (PAA is *N*-phenylanthranilic acid) (Ros *et al.*, 2002). Here, NPA was found to interact with the rhodium center *via* both the amine and carboxyl groups. Recent reports of NPA ligands coordinated to the lanthanides samarium, europium, and gadolinium in a search for novel antibacterial complexes provide several examples of NPA complexes in which the ligand is coordinated to two or three metal centers (Zapała *et al.*, 2019). Analysis of the complexes revealed that NPA coordinates to all of these lanthanides only *via* the carboxylate group. Similar NPA coordination was reported in terbium complexes for luminescence studies (Fu *et al.*, 2008).

Among the first NPA complexes with 3*d* transition metals reported were with Cu^{II} metal centers in tetrakis[μ-2-(phenylamino)benzoato-κ^2O,O']bis[(ethanol)copper(II)] and bis[μ-2-(phenylamino)benzoato-κ^2O,O']bis[(hydroxido)copper(II)] (Taş *et al.*, 2010). Both of these complexes contain two copper centers, with NPA ligands that bridge between the two Cu^{II} centers *via* the carboxylate groups. Mononuclear metal complexes of NPA were reported for Cd and Zn with an additional 2,2′-bipyridine or 3,5-dimethylpyrazole ligand, and for Mn with an additional phenanthroline ligand (Jin & Wang, 2014; Tan *et al.*, 2015).

Little attention has been focused on pharmaceutical agents and coordination compounds of NPA with Zn in a polynuclear motif, although several studies involving trinuclear zinc complexes with a variety of ligands have been reported (Liu *et al.*, 2013; Yu *et al.*, 2007; Neels & Stoeckli-Evans, 1999; Akine *et al.*, 2004; Karmakar *et al.*, 2019; Diop *et al.*, 2014). A recurring theme in this area of research is the exploration of photoluminescence (Fu *et al.*, 2008) and applications in DNA intercalation (Biswas *et al.*, 2014).

In this article, the synthesis and structural characterization of a trinuclear Zn complex with NPA ligands is reported (Scheme 1). The complex was analyzed using NMR and single-crystal X-ray diffraction to confirm the NPA coordination and structural motifs. Docking studies with SARS-COV-2 were conducted to probe the potential for the new complex to act as an antiviral agent.

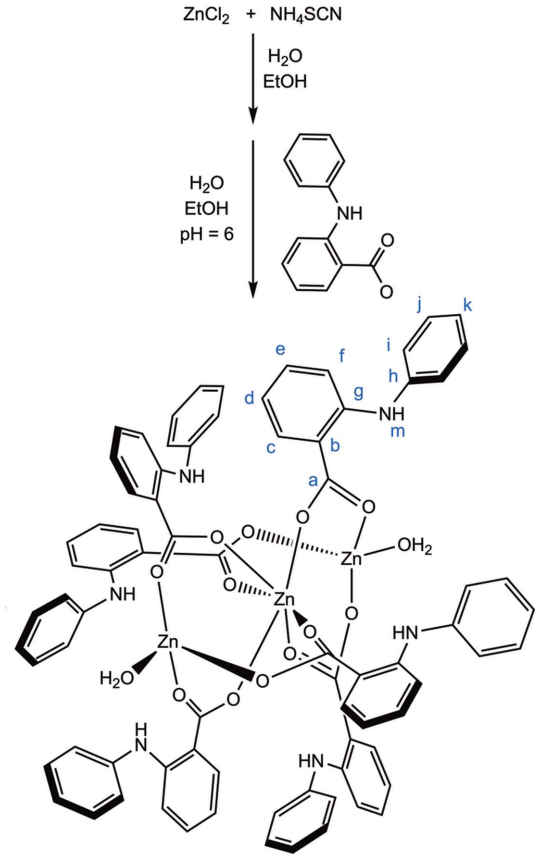

Scheme 1

2. Experimental

All procedures were conducted on the bench in the presence of air and moisture, and all reagents were obtained commercially and used without further purification. Elemental analysis for C, H, and N was conducted using a Costech ECS 4010 CHNSO analyzer. ^{1}H and ^{13}C NMR were conducted using a Varian 400 MHz spectrometer and calibrated to residual dimethyl sulfoxide (DMSO). Associated NMR data (Brannon *et al.*, 2021) and molecular docking data (Mbani *et al.*, 2021) were deposited on *Zenodo* (https://zenodo.org/).

2.1. Synthesis and crystallization of $(NPA)_6Zn_3(H_2O)_2$

$ZnCl_2$ (0.272 g, 0.002 mol) and NH_4SCN (0.144 g, 0.002 mol) were dissolved in a water–ethanol solution (~10 ml, 1:5 *v*/*v*) and placed in a 100 ml Erlenmeyer flask with stirring at room temperature for about 30 min. To this solution was added an ethanolic solution (20 ml) of NPA (0.426 g, 0.002 mol). The pH of the resulting solution was adjusted to about 6 using 10% Et_3N solution and stirring was continued for 24 h. A transparent crystalline complex was obtained from the solution

Table 1
Experimental details.

Crystal data	
Chemical formula	$[Zn_3(C_{13}H_{10}NO_2)_6(H_2O)_2]$
M_r	1505.46
Crystal system, space group	Triclinic, $P\overline{1}$
Temperature (K)	100
a, b, c (Å)	11.0968 (5), 12.8319 (6), 13.3134 (6)
α, β, γ (°)	111.703 (2), 108.028 (2), 93.125 (2)
V (Å^3)	1643.97 (13)
Z	1
Radiation type	Mo $K\alpha$
μ (mm^{-1})	1.16
Crystal size (mm)	0.3 × 0.1 × 0.03
Data collection	
Diffractometer	Bruker Kappa Venture D8
Absorption correction	Multi-scan (*SADABS*; Bruker, 2017)
T_{min}, T_{max}	0.664, 0.748
No. of measured, independent and observed [$I > 2\sigma(I)$] reflections	86106, 10025, 8556
R_{int}	0.044
(sin $\theta/\lambda)_{max}$ (Å^{-1})	0.714
Refinement	
$R[F^2 > 2\sigma(F^2)]$, $wR(F^2)$, S	0.030, 0.078, 1.03
No. of reflections	10025
No. of parameters	477
H-atom treatment	H atoms treated by a mixture of independent and constrained refinement
$\Delta\rho_{max}$, $\Delta\rho_{min}$ (e Å^{-3})	0.65, −0.85

Computer programs: *APEX3* (Bruker, 2017), *SAINT* (Bruker, 2017), *SHELXT* (Sheldrick, 2015*a*), *SHELXL2017* (Sheldrick, 2015*b*), *Mercury* (Macrae *et al.*, 2020), and *OLEX2* (Dolomanov *et al.*, 2009).

(yield 0.273 g, 54%, based on NPA) by slow evaporation for several days, producing crystals suitable for X-ray analysis. Analysis calculated (%) for $C_{78}H_{64}N_6O_{14}Zn_3$: C 62.23, H 4.28, N 5.58; found: C 62.04, 3.83 H, N 5.67. ^{1}H NMR (399.777 MHz, DMSO-d_6, 295 K): δ 6.80 (*m*, 1H; H_d), 7.02 (*t*, J = 8.0 Hz, 1H; H_k), 7.22 (*d*, J = 8.0 Hz, 2H; H_i), 7.33 (*m*, 4H; H_e, H_f, H_j), 8.03 (*d*, J = 8.0 Hz, 1H; H_c), 10.42 (*br s*, 1H; H_m). ^{13}C NMR (100.535 MHz, DMSO-d_6, 295 K): δ 113.7 (C_f), 117.5 (C_d), 117.7 (C_b), 120.2 (C_i), 122.1 (C_k), 129.7 (C_j), 132.5 (C_e), 132.9 (C_c), 141.8 (C_h), 146.0 (C_g), 173.3 (C_a).

2.2. Crystallographic details

Crystal data, data collection and structure refinement details are summarized in Table 1. H atoms were placed at ideal positions excluding the H atoms on the solvent water molecules and nitrogen, which were placed manually at q-peaks.

2.3. Molecular docking

Molecular docking studies were conducted with *AutoDock* (Version 4.2; Trott & Olson, 2010) and *CB-Dock* (Liu *et al.*, 2020; Cao & Li, 2014). The three-dimensional (3D) structure of the main protease (M^{pro}) of SARS-COV-2 (PDB ID: 6lu7) was reported previously with a bound N3 Michael addition inhibitor (Jin *et al.*, 2020). The N3 inhibitor, water molecules, and cocrystallized ligands were removed from the .pdb file prior to commencing docking studies with the new structural coordinates of $(NPA)_6Zn_3(H_2O)_2$. Preparation of the com-

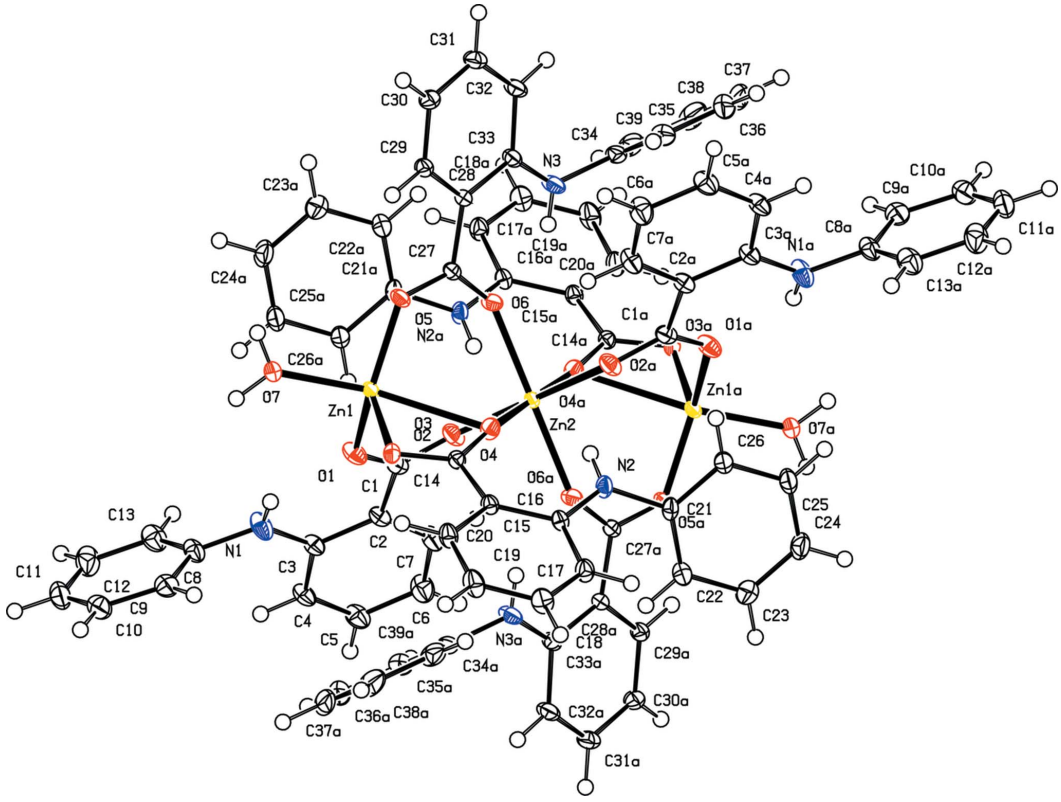

Figure 1
View of $(NPA)_6Zn_3(H_2O)_2$, drawn with 50% probability displacement ellipsoids. [Symmetry code: (a) $-x + 1, -y + 1, -z + 1$.]

pounds and proteins, polar H atoms, and partial charges (Kollman charges) were performed using *AutoDock Tools* (Version 1.5.6) that saved them as a .pdbqt file. *AutoDock Vina* (Version 1.1.2) was used with grid box center values at x = −26.283, y = 12.599, and z = 58.966, and offset values of 62, 126, and 92, respectively. The 3D results of the interactions between the target and compound were analyzed and illustrated with the software *Discovery Studio* (Version 17.2) and *Chimera* (Pettersen *et al.*, 2004).

3. Results and discussion

$(NPA)_6Zn_3(H_2O)_2$ was synthesized from equimolar amounts of $ZnCl_2$ and NH_4SCN, followed by the addition of NPA, and adjusting the pH to 6 with triethylamine. Slow evaporation yielded transparent crystals in 54% yield that were characterized by ^1H, ^{13}C, COSY (correlated spectroscopy), HMBC (heteronuclear multiple bond correlation), and HSQC (heteronuclear single quantum coherence) NMR spectroscopy. The ^1H NMR spectrum in DMSO-d_6 revealed nine protons from the arene groups in the range 6.5–7.8 ppm, with the N—H proton found at 10.40 ppm. The observed signals are shifted from the free amino acid resonances at 6.5–7.4 ppm for the arene protons and 9.31 ppm for the N—H proton (Saito *et al.*, 2018), supporting coordination.

Crystallographic analysis reveals that $(NPA)_6Zn_3(H_2O)_2$ crystallizes in the triclinic space group $P\overline{1}$ and no solvent molecules are found to be trapped in the structure (Fig. 1). The structure is centrosymmetric, with the Zn2 atom located on an inversion center. The asymmetric unit contains two Zn centers (Zn1 and Zn2), about which three NPA ligands and one H_2O ligand are coordinated. The full molecule fills the unit cell, which contains three Zn atoms, six coordinated NPA ligands, and two coordinated terminal H_2O ligands.

The central Zn^{II} atom, Zn2, is hexacoordinated exclusively by O atoms from the carboxylate groups of the NPA ligands. This central Zn^{II} atom has an approximately octahedral molecular geometry, with bond angles ranging from 83.78 (4)° for O2—Zn2—O4^i to 96.22 (4)° for O2—Zn2—O4 [symmetry code: (i) $-x+1, -y+1, -z+1$]. The ligand bond lengths range from 2.0219 (11) Å for Zn2—O2, to 2.0775 (10) Å for Zn2—O6, to 2.1762 (10) Å for Zn2—O4. The N atoms of the NPA ligands are not found to be involved in any coordination interaction with the Zn^{II} centers, which is consistent with predictions from hard–soft acid–base theory (HSAB). However, the H atoms on the N atoms are involved in intramolecular hydrogen bonding with the carboxylate O atoms of NPA (Fig. 2). The hydrogen-bond distances within the asymmetric unit were all around a similar length, with distances of

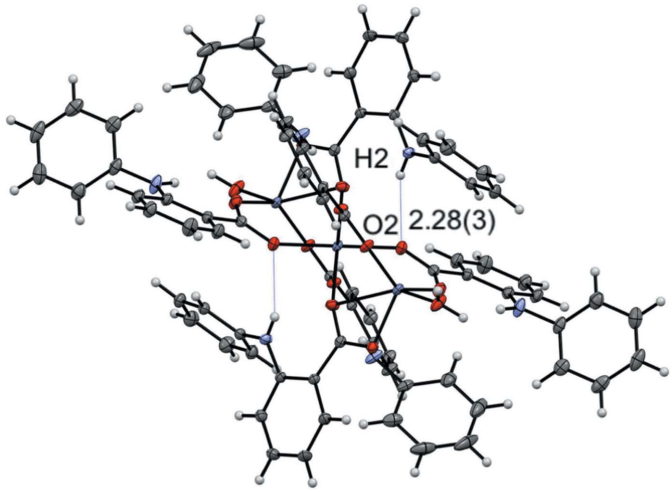

Figure 3
View of $(NPA)_6Zn_3(H_2O)_2$, drawn with 50% probability displacement ellipsoids, highlighting the intramolecular hydrogen bonding. The distances is in Å.

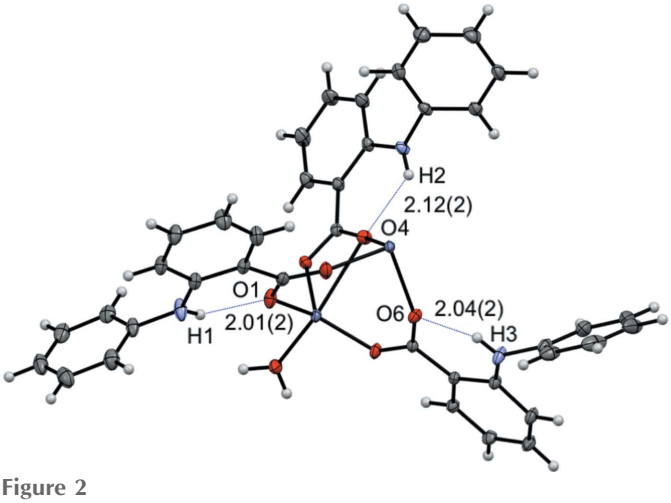

Figure 2
View of half the asymmetric unit of $(NPA)_6Zn_3(H_2O)_2$, drawn with 50% probability displacement ellipsoids, highlighting the intramolecular hydrogen bonding. Distances are in Å.

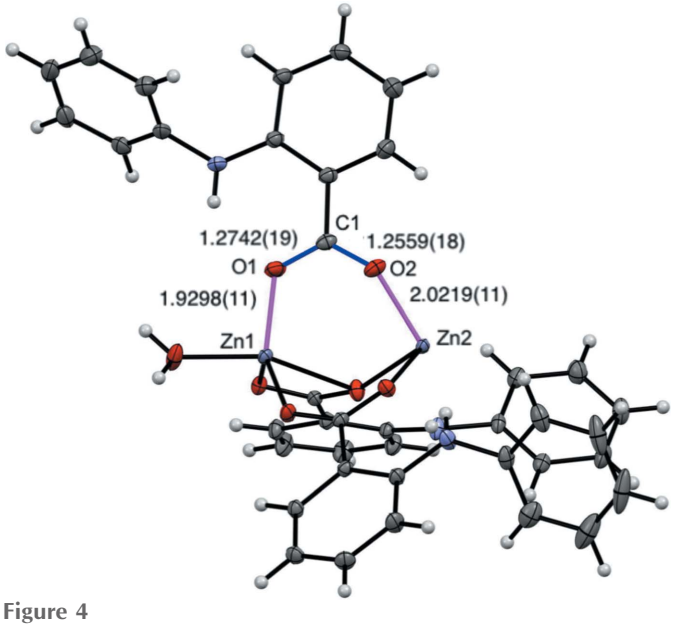

Figure 4
View of half the asymmetric unit of $(NPA)_6Zn_3(H_2O)_2$, drawn with 50% probability displacement ellipsoids, highlighting the Zn—O and carboxylate bond distances (Å).

2.01 (2) Å for O1···H1, 2.12 (2) Å for O4···H2, and 2.04 (2) Å for O6···H3. However, it should be noted that H atoms were fixed, or placed at calculated positions, which will affect the hydrogen-bond distances. Intramolecular hydrogen bonding between the two symmetry-generated halves of the molecule was found between H2 and O2^{i} with a distance of 2.28 (3) Å (Fig. 3).

The exterior Zn^{II} centers Zn1 and Zn1^{i} are penta-coordinated, with only O atoms coordinated to these centers. The Zn1—O bond lengths are generally shorter than the Zn2—O bond lengths, with Zn1—O1 at 1.9298 (11) Å, Zn1—O3 at 1.9920 (10) Å, and Zn1—O5 at 1.9063 (10) Å. However, the notable outlier is that one of the O atoms coordinated to Zn1 comes from an H_2O ligand, with Zn1—O7 at 2.0274 (12) Å. Because the Zn1 and Zn1^{i} centers are pentacoordinated, there are two modes which can be used to classify their geometry: square pyramidal or trigonal bipyramidal. This distinction is made mathematically by utilizing the Addison parameter (Addison *et al.*, 1984). In this analysis, a trigonal index (τ) is assigned according to the equation $\tau = (\beta - \alpha)/60$, where β and α are the largest angles about the metal center. If the resulting value for τ is closer to 0, the center is classified as having a square pyramidal geometry. Conversely, if τ lies closer to 1, the center is classified as having a trigonal bipyramidal geometry. This analysis for Zn1 and Zn1^{i} yielded the value $\tau = 0.566$, indicating that the molecular geometry of Zn1 and its symmetry-generated counterpart Zn1^{i} are best described as trigonal bipyramidal in nature.

For all three NPA ligands of the asymmetric unit, both of the carboxylate O atoms are involved in coordination to Zn. This indicates that the formal negative charge of the ligand is delocalized between both O atoms instead of being localized on a single O atom. Each of the bond lengths between C and O atoms of the carboxylate groups are statistically different, indicating that the resonance is not shared equally. In all cases, the longer carboxylate C—O bond lengths are found for O atoms that are coordinated to Zn1, while shorter carboxylate C—O bond lengths are found for O atoms that are coordinated to Zn2 (Fig. 4). The longer carboxylate C—O bond lengths for C1—O1 at 1.2742 (19) Å, C14—O3 at 1.2866 (17) Å, and C27—O5 at 1.2788 (17) Å correlate with shorter Zn1—O bond lengths of Zn1—O1 at 1.9298 (11) Å, Zn1—O3 at 1.9920 (10) Å, and Zn1—O5 at 1.9063 (10) Å, respectively. By contrast, the shorter carboxylate C—O bond lengths for C1—O2 at 1.2559 (18) Å, C14—O4 at 1.2572 (17) Å, and C27—O6 at 1.2555 (17) Å correlate with

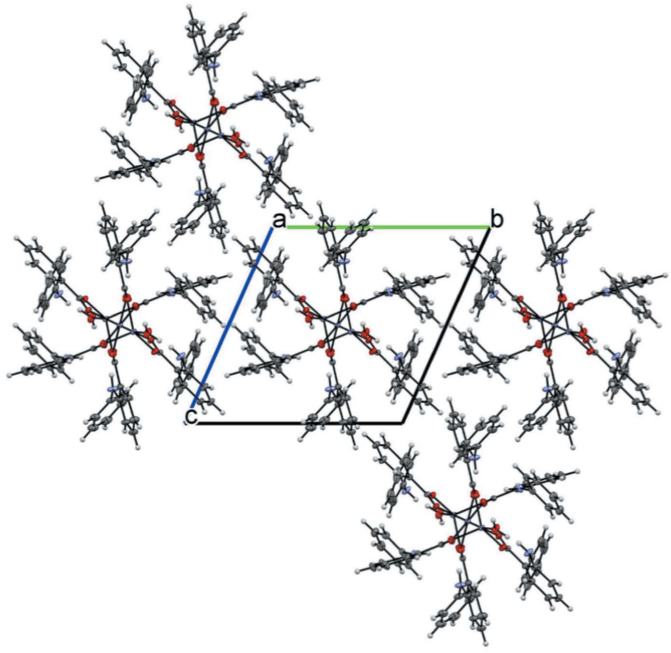

Figure 6
View of the macromolecular packing of $(NPA)_6Zn_3(H_2O)_2$, drawn with 50% probability displacement ellipsoids, viewed along the *c* axis.

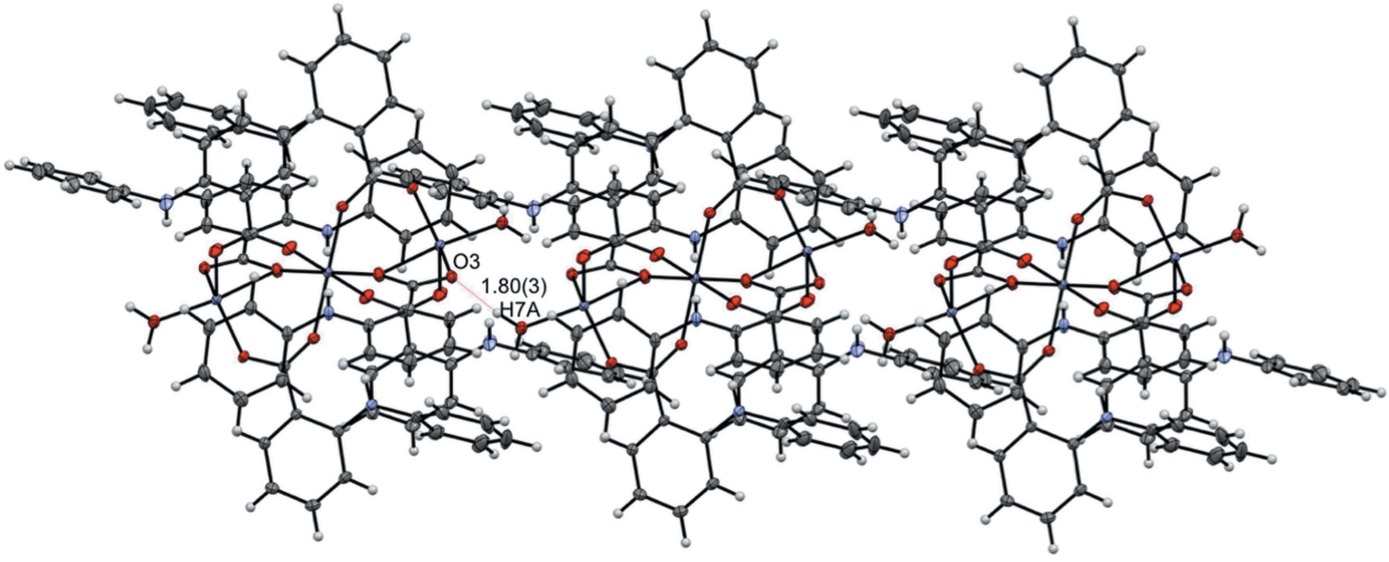

Figure 5
View of three molecules of $(NPA)_6Zn_3(H_2O)_2$, drawn with 50% probability displacement ellipsoids, highlighting the intermolecular hydrogen bonding. The distance is in Å.

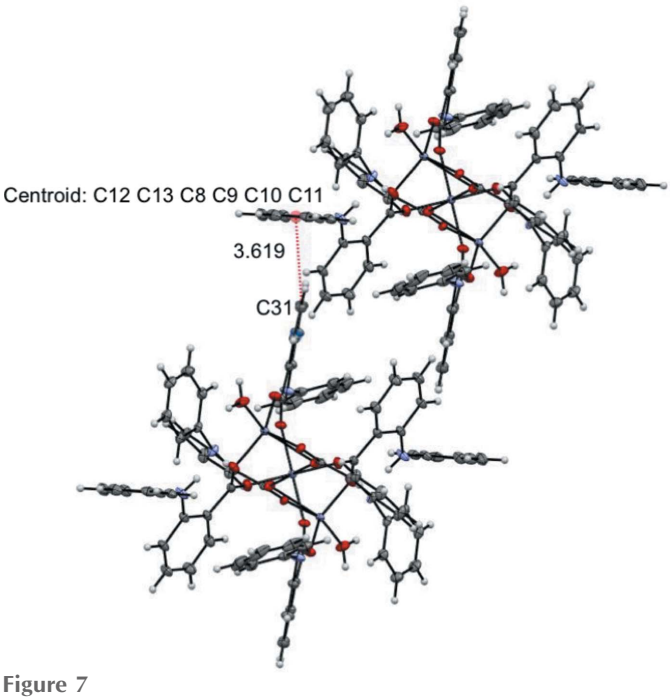

Figure 7
View of two molecules of $(NPA)_6Zn_3(H_2O)_2$, drawn with 50% probability displacement ellipsoids, highlighting the perpendicular π stacking. The distance is in Å.

longer Zn2—O bond lengths of Zn2—O2 at 2.0219 (11) Å, Zn2—O4 at 2.1762 (10) Å, and Zn2—O6 at 2.0775 (10) Å, respectively. The longer Zn2—O bond lengths are likely due to increased steric hindrance around the central Zn2 atom and additional intramolecular hydrogen bonding of the O atoms (O2, O4, and O6) with a neighboring NPA ligand, causing additional torsion and strain (Fig. 3).

The two water ligands are located axially along the complex. Each water ligand is involved in hydrogen bonding from an H atom to a carboxylate O of the next unit cell, with a distance of 1.80 (3) Å for H7*A*···O3. As a result, each complex donates and accepts a hydrogen bond at each end, for a total of four intermolecular hydrogen bonds per molecule. Owing to symmetry-generated elements, it can be seen that all four hydrogen bonds arise from one unique bond (Fig. 5). These intermolecular hydrogen bonds are the main factor determining the arrangement of adjacent complexes. Due to the centrosymmetric nature of the complex and the axial hydrogen bonding, adjacent complexes attach end-on to form rigid straight chains, as shown in Fig. 5. The angle each chain forms is precisely 180°, such that the molecules stack perfectly when viewing a chain of complexes down the *c* axis (Fig. 6).

Multiple chains of the complex are stacked side-by-side (Fig. 7), with the arene groups of the NPA ligands of adjacent complexes in close proximity to one another. Perpendicular π stacking is observed between the centroid defined by atoms C8–C13 and atom C31, with a distance of 3.619 Å and an angle of 83.4° (Fig. 7). π stacking is the primary contact connecting adjacent chains of molecules along the *a* and *b* axes, while hydrogen bonding is the primary contact along the *c* axis.

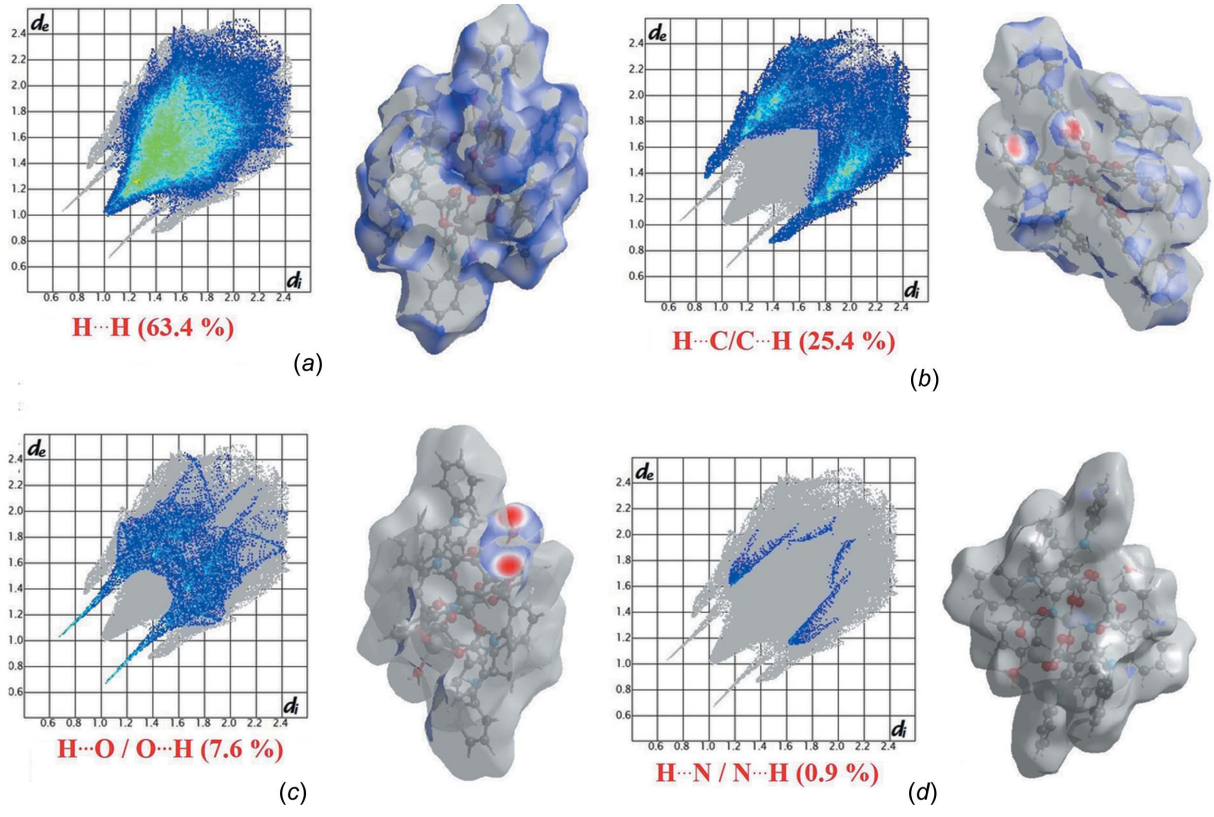

Figure 8
Hirshfeld fingerprint plots for $(NPA)_6Zn_3(H_2O)_2$ with highlighted contributions.

Hirshfeld surface and fingerprint plots were calculated using the *CrystalExplorer* program to further quantify the intermolecular contacts present in the 3D supramolecular architecture of the complex (Spackman & Jayatilaka, 2009; Spackman & McKinnon, 2002). Significant intermolecular interactions are mapped (Fig. 8) that indicate the percentage contributions of the intermolecular contacts to the Hirshfeld surface. Significant contacts include 63.4% H···H, 25.4% H···C/C···H, 7.6% H···O/O···H, and 0.9% H···N/N···H. The largest contribution of 63.4% for H···H interactions has a high concentration at $d_e = d_i \sim 1.02$ Å, as indicated by the red regions [Fig. 8(*a*)]. Two sharp spikes at $d_e + d_i \sim 1.71$ Å were observed for H···O/O···H interactions and indicate strong hydrogen bonding [Fig. 8(*b*)]. For H···C/C···H contacts, two spikes appear at $d_e + d_i \sim 2.25$ Å, while the H···N/N···H contacts have $d_e + d_i \sim 2.8$ Å.

The newly determined structure of $(NPA)_6Zn_3(H_2O)_2$ was used in a molecular docking study with the main protease (M^{pro}) of SARS-COV-2 using *AutoDock* (Version 4.2) and *CB-Dock* to probe the potential utility of $(NPA)_6Zn_3(H_2O)_2$ as an antiviral agent for SARS-COV-2. The structure of M^{pro} (PDB ID: 6lu7) was reported previously with a bound N3 Michael addition inhibitor (Jin *et al.*, 2020) [Fig. 9(*b*)]. The N3 inhibitor, water molecules, and cocrystallized ligands were removed for docking studies with $(NPA)_6Zn_3(H_2O)_2$. Our docking results found the most stable confirmation with a docking score of -8.4 kcal mol^{-1} using *AutoDock* and -8.2 kcal mol^{-1} using *CB-Dock*. This suggests that $(NPA)_6Zn_3(H_2O)_2$ could be a strong inhibitor for M^{pro} because the docking scores are on the same order of magnitude as those reported for Remdesivir at -8.2 kcal mol^{-1} and Baloxavir marboxil at -7.4 kcal mol^{-1} (Naik *et al.*, 2020). The main difference between the docking of $(NPA)_6Zn_3(H_2O)_2$ and Remdesivir is that a different binding location was found for $(NPA)_6Zn_3(H_2O)_2$ [Fig. 9(*b*)]. When using *CB-Dock*, we identified that $(NPA)_6Zn_3(H_2O)_2$ could also bind in the standard binding pocket with a docking score of -6.0 kcal mol^{-1} [Fig. 9(*c*)]. While this is not as favorable a docking score as that of Remdesivir, it is on the same order of magnitude as scores reported for Oseltamivir at -6.1 kcal mol^{-1} and Chloroquine at -5.7 kcal mol^{-1} (Naik *et al.*, 2020). Combined, these results suggest that $(NPA)_6Zn_3(H_2O)_2$ has potential for inhibiting M^{pro} of SARS-CoV-2.

Fig. 9 shows the 3D interaction between $(NPA)_6Zn_3(H_2O)_2$ and M^{pro}, which demonstrates that $(NPA)_6Zn_3(H_2O)_2$ targets a different area of the protein from N3. The strongest binding mode computed at -8.4 kcal mol^{-1} of $(NPA)_6Zn_3(H_2O)_2$ included one hydrogen-bond contact between the $(NPA)_6Zn_3(H_2O)_2$ carboxylate O atom (such as O1) with amino acid residue Gln110 at a distance of 2.72 Å (Fig. 10). However, most of the stabilizing contacts result from π interactions with the benzyl groups (such as C8–C13) in $(NPA)_6Zn_3(H_2O)_2$. Benzyl π···anion contacts were detected with Asp153 at distances of 3.50 and 4.14 Å. Perpendicular π–π stacking was observed with Phe294 at distances of 5.33, 5.37, and 5.01 Å. Benzyl π···alkyl bond contacts were detected with Pro252 at 5.40 Å, Ile249 at 5.18 Å and 5.04 Å, and Val202 at 5.37 Å. Combined, the docking studies support that $(NPA)_6Zn_3$-

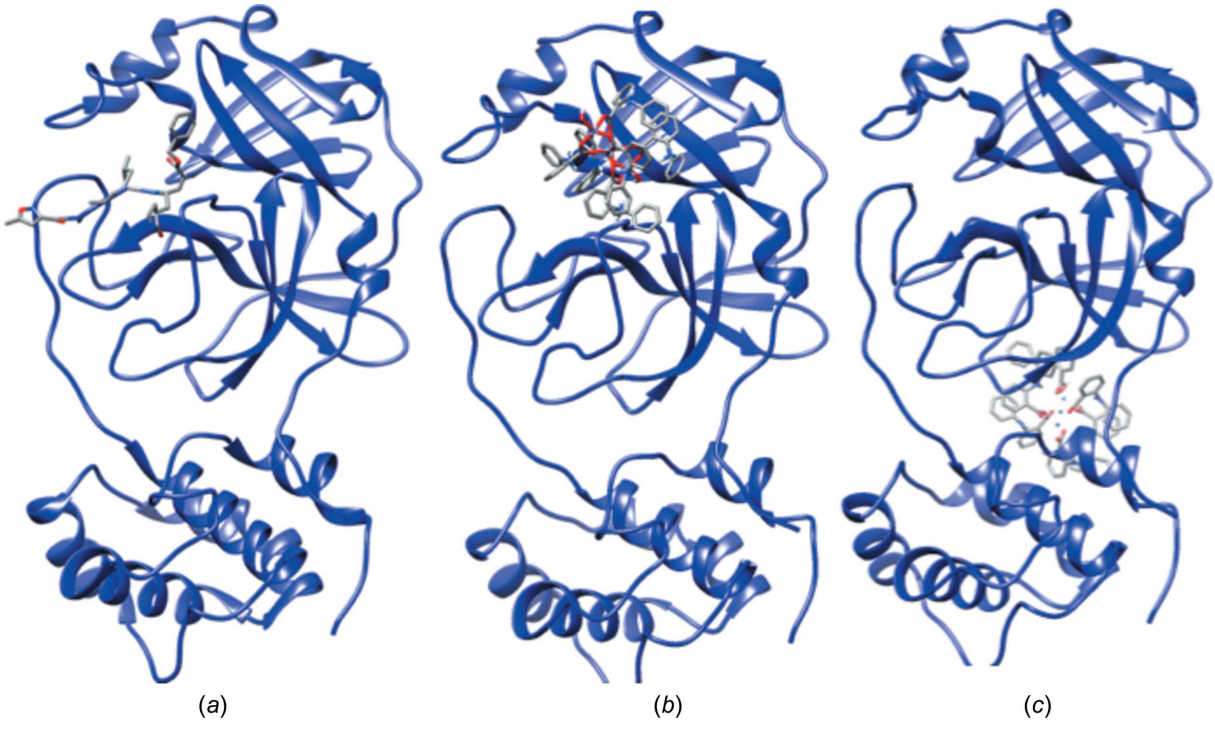

Figure 9
Cartoon representation of M^{pro} with (*a*) the reported N3 inhibitor, (*b*) $(NPA)_6Zn_3(H_2O)_2$ at the standard pocket site and (*c*) $(NPA)_6Zn_3(H_2O)_2$ at the new binding site.

$(H_2O)_2$ could bind to M^{pro} at a different binding site than the most widely studied pocket site in M^{pro} where N3 and Remdesivir are known to bind.

4. Conclusion

The trinuclear zinc complex $(NPA)_6Zn_3(H_2O)_2$ was synthesized and characterized crystallographically. The crystal structure is symmetric about the central Zn^{II} atom (Zn2), which has approximate octahedral geometry, flanked by outer Zn^{II} atoms (Zn2 and Zn2^{i}) with highly contorted trigonal bipyramidal molecular geometries. The macromolecular stabilization is facilitated by intramolecular hydrogen bonding within the NPA ligand, hydrogen bonding between H_2O and carboxylate O atoms of adjacent molecules, and perpendicular π stacking between adjacent molecules. Hydrogen bonding is only observed along the crystallographic *a* axis, while π stacking is only observed along the *b* and *c* axes. Most notably, the supramolecular stabilization results in a perfect alignment of $(NPA)_6Zn_3(H_2O)_2$ molecules along the *a* axis, such that only one molecule is seen when looking down this axis. Molecular docking studies of $(NPA)_6Zn_3(H_2O)_2$ with the M^{pro} portion of SARS-COV-2 suggest that $(NPA)_6Zn_3(H_2O)_2$ could bind to M^{pro} with a similar docking score as Remdesivir, but at a different binding site than the typically targeted pocket site where Remdesivir binds. $(NPA)_6Zn_3(H_2O)_2$ also binds to the same pocket as Remdesivir, with a slightly less favorable docking score, but on the same order of magnitude as other M^{pro} inhibitors. This suggests that trinuclear Zn complexes should be further explored for antiviral activity for SARS-CoV-2.

Acknowledgements

We thank Phil S. Beauchamp for helpful NMR discussions.

Funding information

Funding for this research was provided by: National Science Foundation, Directorate for Mathematical and Physical Sciences (grant No. 1847926 to S. Chantal E. Stieber); U.S.

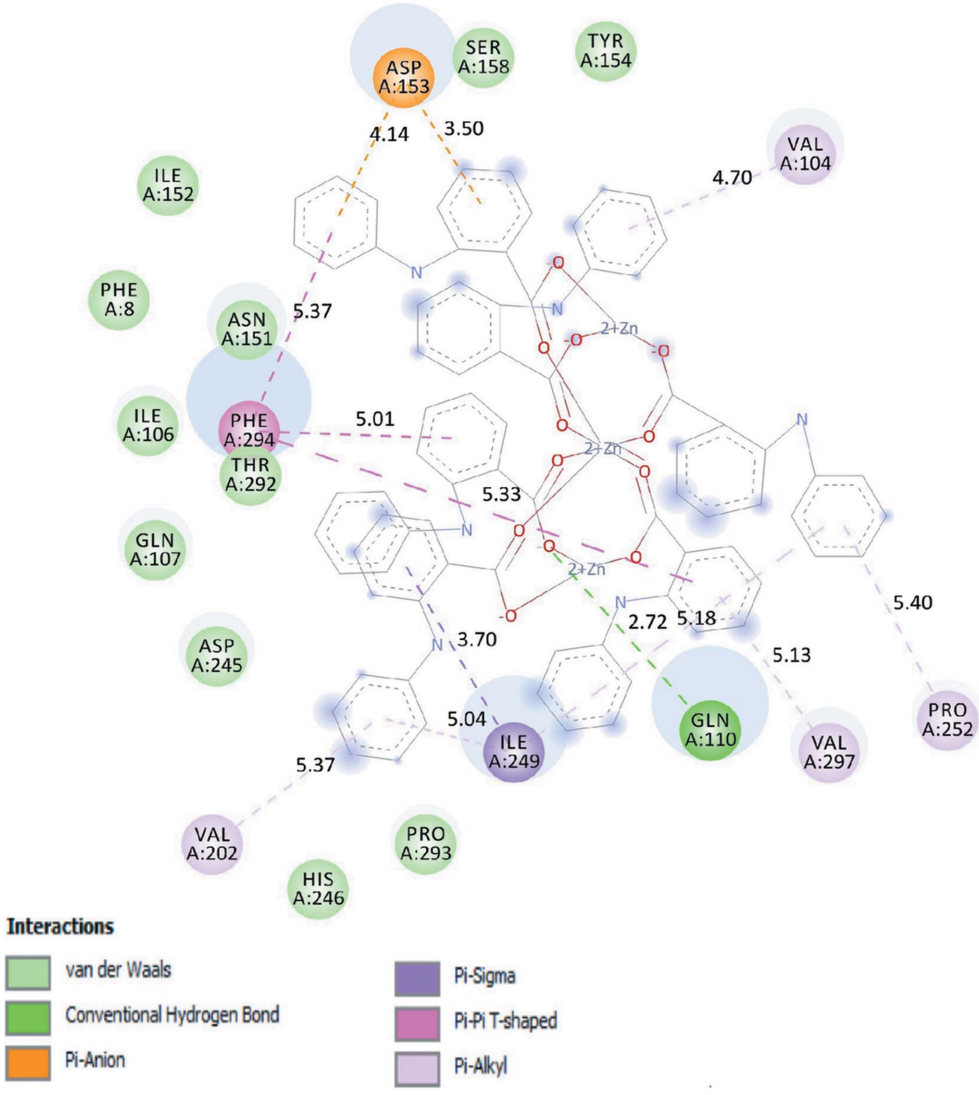

Figure 10
Enlarged view of the newly identified $(NPA)_6Zn_3(H_2O)_2$–M^{pro} binding pocket with the key residue interactions and distances (Å).

Department of Defense, U.S. Army (grant No. W911NF-17-1-0537 to S. Chantal E. Stieber).

References

Addison, A. W., Rao, T. N., Reedijk, J., van Rijn, J. & Verschoor, G. C. (1984). *J. Chem. Soc. Dalton Trans.* pp. 1349–1356.

Aiyelabola, T. O., Isabirye, D. A., Akinkunmi, E. O., Ogunkunle, O. A. & Ojo, I. A. O. (2016). *J. Chem.* **2016**, 7317015.

Akine, S., Taniguchi, T. & Nabeshima, T. (2004). *Inorg. Chem.* **43**, 6142–6144.

Batten, S. R., Neville, S. M. & Tuner, D. R. (2009). In *Coordination Polymers: Design, Analysis and Application*, edited by T. G. House. Cambridge: RSC Publishing.

Beigel, J. H., Tomashek, K. M., Dodd, L. E., Mehta, A. K., Zingman, B. S., Kalil, A. C., Hohmann, E., Chu, H. Y., Luetkemeyer, A., Kline, S., Lopez de Castilla, D., Finberg, R. W., Dierberg, K., Tapson, V., Hsieh, L., Patterson, T. F., Paredes, R., Sweeney, D. A., Short, W. R., Touloumi, G., Lye, D. C., Ohmagari, N., Oh, M. D., Ruiz-Palacios, G. M., Benfield, T., Fätkenheuer, G., Kortepeter, M. G., Atmar, R. L., Creech, C. B., Lundgren, J., Babiker, A. G., Pett, S., Neaton, J. D., Burgess, T. H., Bonnett, T., Green, M., Makowski, M., Osinusi, A., Nayak, S., Lane, H. C. & ACTT-1 Study Group Members (2020). *N. Engl. J. Med.* **383**, 1813–1826.

Biswas, B., Kole, N., Patra, M., Dutta, S. & Ganguly, M. (2014). *J. Chem. Sci.* **125**, 1445–1453.

Brannon, J. P., Gardner-Ricossa, K. D., Mbani, O. A. L., Paboudam, A. G., Agwara, M. O., Bonnand, E. F. & Stieber, S. C. E. (2021). *Zenodo*, doi: 10.5281/zenodo.4694912.

Bruker (2017). *APEX3*, *SAINT*, and *SADABS*. Bruker AXS Inc., Madison, Wisconsin, USA.

Cao, Y. & Li, L. (2014). *Bioinformatics*, **30**, 1674–1680.

Cereda, G., Ciappolino, V., Boscutti, A., Cantu, F., Oldani, L., Delvecchio, G. & Brambilla, P. (2022). *Adv. Nutr.* **13**, 66–79.

Derwand, R. & Scholz, M. (2020). *Med. Hypotheses*, **142**, 109815.

Diop, M., Aly-Gaye, P., Bouyagui-Tamboura, F., Gaye, M., Pérez-Lourido, P., Valencia, L. & Castro, G. (2014). *Z. Anorg. Allg. Chem.* **640**, 1392–1396.

Dolomanov, O. V., Bourhis, L. J., Gildea, R. J., Howard, J. A. K. & Puschmann, H. (2009). *J. Appl. Cryst.* **42**, 339–341.

El-Boraey, H. A. & El-Salamony, M. A. (2019). *J. Inorg. Organomet. Polym.* **29**, 684–700.

Fu, Y., Zhang, J., Lv, Y. & Cao, W. (2008). *Spectrochim. Acta A Mol. Biomol. Spectrosc.* **70**, 646–650.

Jin, S. & Wang, D. (2014). *Inorg. Chim. Acta*, **415**, 31–43.

Jin, Z., Du, X., Xu, Y., Deng, Y., Liu, M., Zhao, Y., Zhang, B., Li, X., Zhang, L., Peng, C., Duan, Y., Yu, J., Wang, L., Yang, K., Liu, F., Jiang, R., Yang, X., You, T., Liu, X., Yang, X., Bai, F., Liu, H., Liu, X., Guddat, L. W., Xu, W., Xiao, G., Qin, C., Shi, Z., Jiang, H., Rao, Z. & Yang, H. (2020). *Nature*, **582**, 289–293.

Karmakar, M., Roy, S. & Chattopadhyay, S. (2019). *New J. Chem.* **43**, 10093–10102.

Liu, X., Du, P. & Cao, R. (2013). *Nat. Commun.* **4**, 2375.

Liu, Y., Grimm, M., Dai, W., Hou, M., Xiao, Z. & Cao, Y. (2020). *Acta Pharmacol. Sin.* **41**, 138–144.

Macrae, C. F., Sovago, I., Cottrell, S. J., Galek, P. T. A., McCabe, P., Pidcock, E., Platings, M., Shields, G. P., Stevens, J. S., Towler, M. & Wood, P. A. (2020). *J. Appl. Cryst.* **53**, 226–235.

Mbani, O. A. L., Paboudam, A. G., Stieber, S. C. E. & Agwara, M. O. (2021). *Zenodo*, doi: 10.5281/zenodo.5703439.

Naik, V. R., Munikumar, M., Ramakrishna, U., Srujana, M., Goudar, G., Naresh, P., Kumar, B. N. & Hemalatha, R. (2020). *J. Biomol. Struct. Dyn.* pp. 2–14.

Neels, A. & Stoeckli-Evans, H. (1999). *Inorg. Chem.* **38**, 6164–6170.

Pettersen, E. F., Goddard, T. D., Huang, C. C., Couch, G. S., Greenblatt, D. M., Meng, E. C. & Ferrin, T. E. (2004). *J. Comput. Chem.* **25**, 1605–1612.

Ros, T. G., van der Lee, M. K., van Dillen, A. J., Geus, J. W. & Koningsberger, D. C. (2002). *J. Mol. Catal. A Chem.* **186**, 13–24.

Saito, T., Yamaji, T., Hayamizu, K., Yanagisawa, M. & Yamamoto, O. (2018). Spectral Database for Organic Compounds SDBS, National Institute of Advanced Industrial Science and Technology (AIST), Japan.

Sheldrick, G. M. (2015*a*). *Acta Cryst.* A**71**, 3–8.

Sheldrick, G. M. (2015*b*). *Acta Cryst.* C**71**, 3–8.

Spackman, M. A. & Jayatilaka, D. (2009). *CrystEngComm*, **11**, 19–32.

Spackman, M. A. & McKinnon, J. J. (2002). *CrystEngComm*, **4**, 378–392.

Tan, Y., Xiong, J., Gao, J., Xu, Q., Fu, C., Tang, Y., Yang, S. & Wen, H. (2015). *J. Mol. Struct.* **1086**, 49–55.

Taş, M., Yeşilel, O. Z. & Büyükgüngör, O. (2010). *J. Inorg. Organomet. Polym.* **20**, 298–305.

te Velthuis, A. J. W., van den Worm, S. H. E., Sims, A. C., Baric, R. S., Snijder, E. J. & van Hemert, M. J. (2010). *PLoS Pathog.* **6**, e1001176.

Trott, O. & Olson, A. J. (2010). *J. Comput. Chem.* **31**, 455–461.

Yu, T., Zhang, K., Zhao, Y., Yang, C., Zhang, H., Fan, D. & Dong, W. (2007). *Inorg. Chem. Commun.* **10**, 401–403.

Zapała, L., Kosińska, M., Woźnicka, E., Byczyński, Ł., Ciszkowicz, E., Lecka-Szlachta, K., Zapała, W. & Chutkowski, M. (2019). *Thermochim. Acta*, **671**, 134–148.

supporting information

Acta Cryst. (2022). C**78**, 231-239 [https://doi.org/10.1107/S205322962200239X]

Synthesis, structural analysis, and docking studies with SARS-CoV-2 of a trinuclear zinc complex with *N*-phenylanthranilic acid ligands

Armel L. Mbani O., Evan F. Bonnand, Awawou G. Paboudam, Jacob P. Brannon, Kevyn D. Gardner-Ricossa, S. Chantal E. Stieber and Moise O. Agwara

Computing details

Data collection: *APEX3* (Bruker, 2017); cell refinement: *SAINT* (Bruker, 2017); data reduction: *SAINT* (Bruker, 2017); program(s) used to solve structure: SHELXT (Sheldrick, 2015*a*); program(s) used to refine structure: *SHELXL2017* (Sheldrick, 2015*b*); molecular graphics: *Mercury* (Macrae *et al.*, 2020); software used to prepare material for publication: OLEX2 (Dolomanov *et al.*, 2009).

Hexakis(μ_2-2-anilinobenzoato)diaquatrizinc(II)

Crystal data

$[Zn_3(C_{13}H_{10}NO_2)_6(H_2O)_2]$
M_r = 1505.46
Triclinic, $P\overline{1}$
a = 11.0968 (5) Å
b = 12.8319 (6) Å
c = 13.3134 (6) Å
α = 111.703 (2)°
β = 108.028 (2)°
γ = 93.125 (2)°
V = 1643.97 (13) Å^3
Z = 1
$F(000)$ = 776
D_x = 1.521 Mg m^{-3}
Mo $K\alpha$ radiation, λ = 0.71073 Å
Cell parameters from 9800 reflections
θ = 2.5–38.9°
μ = 1.16 mm^{-1}
T = 100 K
Prism, clear colourless
0.3 × 0.1 × 0.03 mm

Data collection

Bruker Kappa Venture D8 diffractometer
Radiation source: microfocus sealed X-ray tube, Incoatec Iμs
Mirror optics monochromator
Detector resolution: 7.9 pixels mm^{-1}
ω and φ scans
Absorption correction: multi-scan (SADABS; Bruker, 2017)
T_{min} = 0.664, T_{max} = 0.748
86106 measured reflections
10025 independent reflections
8556 reflections with $I > 2\sigma(I)$
R_{int} = 0.044
θ_{max} = 30.5°, θ_{min} = 2.9°
h = −15→15
k = −18→18
l = −19→19

Refinement

Refinement on F^2
Least-squares matrix: full
$R[F^2 > 2\sigma(F^2)]$ = 0.030
$wR(F^2)$ = 0.078
S = 1.03
10025 reflections
477 parameters
0 restraints
Primary atom site location: dual
Hydrogen site location: mixed
H atoms treated by a mixture of independent and constrained refinement

$w = 1/[\sigma^2(F_o^2) + (0.0319P)^2 + 1.352P]$
where $P = (F_o^2 + 2F_c^2)/3$
$(\Delta/\sigma)_{max} = 0.001$

$\Delta\rho_{max} = 0.65$ e Å^{-3}
$\Delta\rho_{min} = -0.84$ e Å^{-3}

Special details

Geometry. All esds (except the esd in the dihedral angle between two l.s. planes) are estimated using the full covariance matrix. The cell esds are taken into account individually in the estimation of esds in distances, angles and torsion angles; correlations between esds in cell parameters are only used when they are defined by crystal symmetry. An approximate (isotropic) treatment of cell esds is used for estimating esds involving l.s. planes.

Refinement. $(NPA)_6Zn_3(H_2O)_2$ was mounted on a Bruker Kappa Venture D8 instrument on a Kapton sample holder that was then placed in a liquid nitrogen stream to cool the sample down to 100 K. The sample was run with a molybdenum micro source (Mo *Kα*, *λ*= 0.71073 Å) using a Photon II detector. The unit cell of was determined prior to full data collection, and data were integrated using the Bruker SAINT program using SADABS for absorption correction. Structural refinement was conducted using APEX3 and OLEX2 software that interfaced with the SHELXL PC Suite (Dolomanov *et al.*, 2009; Sheldrick, Sheldrick, 2015*b*). All non-H atoms were refined using anisotropic thermal parameters.

Fractional atomic coordinates and isotropic or equivalent isotropic displacement parameters (Å²)

	x	*y*	*z*	U_{iso}*/U_{eq}
Zn1	0.21623 (2)	0.57673 (2)	0.53262 (2)	0.01224 (4)
Zn2	0.500000	0.500000	0.500000	0.01101 (5)
O3	0.18796 (10)	0.46312 (9)	0.59622 (9)	0.01493 (19)
O5	0.33767 (10)	0.71566 (9)	0.63184 (9)	0.0163 (2)
O6	0.50591 (10)	0.67473 (9)	0.57499 (9)	0.0156 (2)
O4	0.38584 (10)	0.46623 (9)	0.59513 (10)	0.0169 (2)
O7	0.05686 (11)	0.64469 (11)	0.54001 (12)	0.0257 (3)
O2	0.34886 (11)	0.47459 (10)	0.35584 (9)	0.0199 (2)
O1	0.15384 (11)	0.48147 (10)	0.36899 (9)	0.0207 (2)
N2	0.52659 (12)	0.32556 (11)	0.66916 (12)	0.0165 (2)
N3	0.70966 (13)	0.84458 (12)	0.65803 (12)	0.0209 (3)
N1	−0.05046 (13)	0.40036 (14)	0.17526 (12)	0.0248 (3)
C29	0.47282 (14)	0.91895 (12)	0.80522 (13)	0.0152 (3)
H29	0.392254	0.886158	0.802241	0.018*
C28	0.52736 (13)	0.85540 (11)	0.72560 (12)	0.0128 (2)
C16	0.41632 (13)	0.28630 (12)	0.68010 (12)	0.0137 (2)
C33	0.64919 (14)	0.90238 (12)	0.73231 (12)	0.0154 (3)
C2	0.16772 (14)	0.37100 (13)	0.18719 (12)	0.0165 (3)
C26	0.75406 (14)	0.31903 (13)	0.72482 (13)	0.0169 (3)
H26	0.771698	0.394102	0.783266	0.020*
C3	0.03344 (14)	0.35001 (13)	0.12401 (12)	0.0169 (3)
C21	0.62687 (14)	0.26427 (13)	0.65586 (13)	0.0153 (3)
C30	0.53243 (15)	1.02765 (12)	0.88784 (13)	0.0175 (3)
H30	0.494528	1.068533	0.941905	0.021*
C32	0.70667 (15)	1.01528 (13)	0.81453 (14)	0.0203 (3)
H32	0.786401	1.049860	0.817622	0.024*
C7	0.24937 (16)	0.31571 (15)	0.13244 (14)	0.0225 (3)
H7	0.339316	0.331356	0.175194	0.027*
C17	0.41055 (15)	0.19384 (13)	0.71268 (14)	0.0183 (3)
H17	0.481000	0.154891	0.720440	0.022*

C22	0.60164 (15)	0.15393 (14)	0.57133 (14)	0.0201 (3)
H22	0.515144	0.116452	0.523614	0.024*
C19	0.19940 (15)	0.21460 (15)	0.72331 (15)	0.0228 (3)
H19	0.127418	0.191002	0.739352	0.027*
C18	0.30479 (16)	0.15924 (15)	0.73335 (15)	0.0218 (3)
H18	0.303180	0.096516	0.754887	0.026*
C20	0.20171 (14)	0.30396 (14)	0.68974 (13)	0.0182 (3)
H20	0.130606	0.342222	0.683176	0.022*
C15	0.30715 (13)	0.33982 (12)	0.66494 (12)	0.0138 (2)
C25	0.85502 (15)	0.26398 (14)	0.70820 (15)	0.0215 (3)
H25	0.941724	0.302140	0.754172	0.026*
C34	0.84477 (15)	0.86983 (13)	0.68544 (15)	0.0193 (3)
C14	0.29532 (13)	0.42742 (12)	0.61725 (12)	0.0129 (2)
C31	0.64947 (15)	1.07621 (13)	0.89027 (14)	0.0201 (3)
H31	0.690087	1.151989	0.944656	0.024*
C4	−0.01196 (15)	0.27355 (14)	0.00644 (13)	0.0195 (3)
H4	−0.101030	0.259682	−0.038487	0.023*
C27	0.45353 (13)	0.74034 (12)	0.63763 (12)	0.0129 (2)
C24	0.82974 (16)	0.15365 (15)	0.62484 (16)	0.0247 (3)
H24	0.898868	0.115683	0.614252	0.030*
C1	0.22793 (14)	0.44702 (12)	0.31205 (12)	0.0161 (3)
C23	0.70285 (17)	0.09865 (15)	0.55673 (16)	0.0248 (3)
H23	0.685355	0.022754	0.499856	0.030*
C5	0.07081 (16)	0.21858 (15)	−0.04435 (13)	0.0224 (3)
H5	0.037349	0.165888	−0.123144	0.027*
C35	0.93108 (17)	0.88179 (14)	0.79226 (17)	0.0273 (4)
H35	0.899654	0.873909	0.848340	0.033*
C9	−0.27061 (16)	0.33864 (14)	0.15414 (14)	0.0224 (3)
H9	−0.238626	0.311924	0.213239	0.027*
C8	−0.18516 (15)	0.38650 (14)	0.11840 (13)	0.0207 (3)
C6	0.20304 (17)	0.23893 (16)	0.01791 (15)	0.0268 (3)
H6	0.259623	0.200922	−0.017628	0.032*
C10	−0.40284 (17)	0.32986 (15)	0.10340 (16)	0.0274 (4)
H10	−0.460956	0.299287	0.129504	0.033*
C39	0.89097 (18)	0.88128 (14)	0.60371 (17)	0.0258 (3)
H39	0.832464	0.873032	0.530741	0.031*
C13	−0.23263 (17)	0.42410 (16)	0.03090 (15)	0.0265 (3)
H13	−0.174607	0.457781	0.006907	0.032*
C11	−0.44982 (17)	0.36558 (17)	0.01499 (16)	0.0312 (4)
H11	−0.540240	0.358033	−0.020802	0.037*
C12	−0.36467 (18)	0.41245 (18)	−0.02135 (16)	0.0309 (4)
H12	−0.396992	0.436662	−0.082321	0.037*
C36	1.06257 (19)	0.90516 (17)	0.8164 (2)	0.0407 (5)
H36	1.121435	0.913366	0.889251	0.049*
C38	1.0236 (2)	0.90494 (16)	0.6292 (2)	0.0392 (5)
H38	1.055534	0.913039	0.573478	0.047*
C37	1.10874 (19)	0.91665 (17)	0.7347 (3)	0.0463 (6)
H37	1.199117	0.932597	0.751558	0.056*

H3	0.671 (2)	0.7818 (19)	0.6117 (19)	0.022 (5)*
H2	0.533 (2)	0.386 (2)	0.6618 (19)	0.028 (6)*
H1	−0.023 (2)	0.436 (2)	0.247 (2)	0.030 (6)*
H7A	−0.026 (3)	0.615 (2)	0.494 (3)	0.055 (8)*
H7B	0.059 (3)	0.714 (3)	0.578 (2)	0.050 (8)*

Atomic displacement parameters (Å²)

	U^{11}	U^{22}	U^{33}	U^{12}	U^{13}	U^{23}
Zn1	0.00879 (7)	0.01233 (8)	0.01258 (8)	−0.00010 (5)	0.00274 (6)	0.00297 (6)
Zn2	0.00780 (10)	0.01103 (10)	0.01193 (10)	0.00122 (7)	0.00275 (8)	0.00293 (8)
O3	0.0114 (4)	0.0154 (5)	0.0185 (5)	0.0039 (4)	0.0047 (4)	0.0077 (4)
O5	0.0103 (4)	0.0150 (5)	0.0184 (5)	−0.0016 (4)	0.0047 (4)	0.0020 (4)
O6	0.0153 (5)	0.0124 (4)	0.0168 (5)	−0.0005 (4)	0.0075 (4)	0.0025 (4)
O4	0.0158 (5)	0.0182 (5)	0.0230 (5)	0.0051 (4)	0.0110 (4)	0.0115 (4)
O7	0.0115 (5)	0.0166 (5)	0.0392 (7)	0.0030 (4)	0.0039 (5)	0.0049 (5)
O2	0.0152 (5)	0.0220 (5)	0.0175 (5)	−0.0016 (4)	−0.0004 (4)	0.0084 (4)
O1	0.0172 (5)	0.0243 (6)	0.0132 (5)	−0.0028 (4)	0.0022 (4)	0.0032 (4)
N2	0.0115 (5)	0.0190 (6)	0.0252 (6)	0.0053 (5)	0.0086 (5)	0.0135 (5)
N3	0.0144 (6)	0.0165 (6)	0.0230 (6)	−0.0039 (5)	0.0095 (5)	−0.0027 (5)
N1	0.0155 (6)	0.0360 (8)	0.0114 (6)	0.0019 (6)	0.0021 (5)	0.0001 (6)
C29	0.0127 (6)	0.0144 (6)	0.0173 (6)	0.0016 (5)	0.0061 (5)	0.0047 (5)
C28	0.0108 (6)	0.0115 (6)	0.0136 (6)	0.0007 (5)	0.0027 (5)	0.0039 (5)
C16	0.0107 (6)	0.0174 (6)	0.0140 (6)	0.0024 (5)	0.0044 (5)	0.0076 (5)
C33	0.0118 (6)	0.0147 (6)	0.0162 (6)	−0.0003 (5)	0.0048 (5)	0.0029 (5)
C2	0.0149 (6)	0.0177 (6)	0.0136 (6)	−0.0009 (5)	0.0028 (5)	0.0054 (5)
C26	0.0138 (6)	0.0192 (7)	0.0198 (7)	0.0035 (5)	0.0055 (5)	0.0107 (6)
C3	0.0145 (6)	0.0192 (7)	0.0137 (6)	−0.0004 (5)	0.0036 (5)	0.0049 (5)
C21	0.0120 (6)	0.0200 (7)	0.0202 (7)	0.0062 (5)	0.0078 (5)	0.0126 (6)
C30	0.0179 (7)	0.0146 (6)	0.0170 (6)	0.0030 (5)	0.0069 (5)	0.0025 (5)
C32	0.0150 (7)	0.0159 (7)	0.0227 (7)	−0.0037 (5)	0.0065 (6)	0.0012 (6)
C7	0.0152 (7)	0.0283 (8)	0.0194 (7)	0.0011 (6)	0.0036 (6)	0.0074 (6)
C17	0.0150 (6)	0.0216 (7)	0.0225 (7)	0.0048 (5)	0.0064 (5)	0.0137 (6)
C22	0.0141 (6)	0.0226 (7)	0.0221 (7)	0.0035 (6)	0.0045 (6)	0.0092 (6)
C19	0.0158 (7)	0.0331 (9)	0.0286 (8)	0.0032 (6)	0.0106 (6)	0.0203 (7)
C18	0.0192 (7)	0.0263 (8)	0.0273 (8)	0.0036 (6)	0.0082 (6)	0.0190 (7)
C20	0.0135 (6)	0.0250 (7)	0.0213 (7)	0.0047 (5)	0.0083 (5)	0.0132 (6)
C15	0.0117 (6)	0.0161 (6)	0.0151 (6)	0.0023 (5)	0.0055 (5)	0.0074 (5)
C25	0.0120 (6)	0.0263 (8)	0.0285 (8)	0.0047 (6)	0.0057 (6)	0.0148 (7)
C34	0.0147 (7)	0.0127 (6)	0.0292 (8)	0.0004 (5)	0.0109 (6)	0.0048 (6)
C14	0.0115 (6)	0.0139 (6)	0.0118 (6)	0.0025 (5)	0.0044 (5)	0.0035 (5)
C31	0.0190 (7)	0.0144 (6)	0.0192 (7)	−0.0009 (5)	0.0047 (6)	0.0008 (5)
C4	0.0152 (7)	0.0232 (7)	0.0136 (6)	−0.0021 (6)	0.0028 (5)	0.0033 (6)
C27	0.0112 (6)	0.0130 (6)	0.0128 (6)	0.0006 (5)	0.0029 (5)	0.0048 (5)
C24	0.0183 (7)	0.0272 (8)	0.0349 (9)	0.0108 (6)	0.0135 (7)	0.0151 (7)
C1	0.0168 (7)	0.0149 (6)	0.0145 (6)	−0.0004 (5)	0.0021 (5)	0.0069 (5)
C23	0.0225 (8)	0.0220 (7)	0.0297 (8)	0.0072 (6)	0.0112 (7)	0.0084 (7)
C5	0.0206 (7)	0.0264 (8)	0.0135 (6)	−0.0002 (6)	0.0048 (6)	0.0025 (6)

C35	0.0219 (8)	0.0187 (7)	0.0367 (9)	0.0010 (6)	0.0053 (7)	0.0110 (7)
C9	0.0220 (7)	0.0215 (7)	0.0176 (7)	0.0034 (6)	0.0087 (6)	0.0003 (6)
C8	0.0146 (7)	0.0243 (7)	0.0136 (6)	0.0016 (6)	0.0038 (5)	−0.0011 (6)
C6	0.0212 (8)	0.0337 (9)	0.0211 (8)	0.0064 (7)	0.0088 (6)	0.0052 (7)
C10	0.0193 (8)	0.0256 (8)	0.0283 (8)	0.0018 (6)	0.0116 (7)	−0.0009 (7)
C39	0.0270 (8)	0.0187 (7)	0.0393 (10)	0.0077 (6)	0.0219 (8)	0.0112 (7)
C13	0.0227 (8)	0.0318 (9)	0.0191 (7)	0.0023 (7)	0.0061 (6)	0.0056 (7)
C11	0.0163 (7)	0.0332 (9)	0.0279 (9)	0.0066 (7)	0.0037 (6)	−0.0018 (7)
C12	0.0258 (9)	0.0375 (10)	0.0207 (8)	0.0102 (7)	0.0028 (7)	0.0065 (7)
C36	0.0194 (8)	0.0237 (9)	0.0672 (15)	0.0031 (7)	−0.0011 (9)	0.0195 (9)
C38	0.0336 (10)	0.0251 (9)	0.0799 (16)	0.0133 (8)	0.0415 (11)	0.0253 (10)
C37	0.0161 (8)	0.0241 (9)	0.105 (2)	0.0072 (7)	0.0233 (11)	0.0304 (11)

Geometric parameters (Å, º)

Zn1—O3	1.9920 (10)	C7—H7	0.9500
Zn1—O5	1.9063 (10)	C7—C6	1.381 (2)
Zn1—O7	2.0274 (12)	C17—H17	0.9500
Zn1—O1	1.9298 (11)	C17—C18	1.372 (2)
Zn2—O6^{i}	2.0775 (10)	C22—H22	0.9500
Zn2—O6	2.0775 (10)	C22—C23	1.386 (2)
Zn2—O4^{i}	2.1762 (10)	C19—H19	0.9500
Zn2—O4	2.1762 (10)	C19—C18	1.398 (2)
Zn2—O2	2.0219 (11)	C19—C20	1.378 (2)
Zn2—O2^{i}	2.0219 (11)	C18—H18	0.9500
O3—C14	1.2866 (17)	C20—H20	0.9500
O5—C27	1.2788 (17)	C20—C15	1.4080 (19)
O6—C27	1.2555 (17)	C15—C14	1.4752 (19)
O4—C14	1.2572 (17)	C25—H25	0.9500
O7—H7A	0.90 (3)	C25—C24	1.384 (2)
O7—H7B	0.84 (3)	C34—C35	1.394 (3)
O2—C1	1.2559 (18)	C34—C39	1.387 (2)
O1—C1	1.2742 (19)	C31—H31	0.9500
N2—C16	1.3674 (18)	C4—H4	0.9500
N2—C21	1.4151 (18)	C4—C5	1.379 (2)
N2—H2	0.81 (2)	C24—H24	0.9500
N3—C33	1.3787 (19)	C24—C23	1.390 (2)
N3—C34	1.4166 (19)	C23—H23	0.9500
N3—H3	0.80 (2)	C5—H5	0.9500
N1—C3	1.372 (2)	C5—C6	1.398 (2)
N1—C8	1.418 (2)	C35—H35	0.9500
N1—H1	0.83 (2)	C35—C36	1.383 (3)
C29—H29	0.9500	C9—H9	0.9500
C29—C28	1.4024 (19)	C9—C8	1.391 (2)
C29—C30	1.381 (2)	C9—C10	1.391 (2)
C28—C33	1.4126 (19)	C8—C13	1.389 (2)
C28—C27	1.4893 (19)	C6—H6	0.9500
C16—C17	1.410 (2)	C10—H10	0.9500

C16—C15	1.4220 (19)	C10—C11	1.383 (3)
C33—C32	1.414 (2)	C39—H39	0.9500
C2—C3	1.419 (2)	C39—C38	1.393 (3)
C2—C7	1.397 (2)	C13—H13	0.9500
C2—C1	1.484 (2)	C13—C12	1.386 (2)
C26—H26	0.9500	C11—H11	0.9500
C26—C21	1.393 (2)	C11—C12	1.387 (3)
C26—C25	1.388 (2)	C12—H12	0.9500
C3—C4	1.410 (2)	C36—H36	0.9500
C21—C22	1.390 (2)	C36—C37	1.387 (4)
C30—H30	0.9500	C38—H38	0.9500
C30—C31	1.395 (2)	C38—C37	1.377 (4)
C32—H32	0.9500	C37—H37	0.9500
C32—C31	1.378 (2)		

O3—Zn1—O7	97.20 (5)	C18—C19—H19	120.6
O5—Zn1—O3	118.92 (5)	C20—C19—H19	120.6
O5—Zn1—O7	95.94 (5)	C20—C19—C18	118.87 (14)
O5—Zn1—O1	135.15 (5)	C17—C18—C19	121.21 (14)
O1—Zn1—O3	101.15 (5)	C17—C18—H18	119.4
O1—Zn1—O7	98.30 (5)	C19—C18—H18	119.4
O6^{i}—Zn2—O6	180.0	C19—C20—H20	119.3
O6^{i}—Zn2—O4	87.99 (4)	C19—C20—C15	121.44 (14)
O6—Zn2—O4	92.00 (4)	C15—C20—H20	119.3
O6—Zn2—O4^{i}	88.00 (4)	C16—C15—C14	122.83 (12)
O6^{i}—Zn2—O4^{i}	92.00 (4)	C20—C15—C16	119.33 (13)
O4^{i}—Zn2—O4	180.00 (4)	C20—C15—C14	117.73 (13)
O2^{i}—Zn2—O6^{i}	93.86 (4)	C26—C25—H25	119.9
O2—Zn2—O6^{i}	86.14 (4)	C24—C25—C26	120.20 (15)
O2^{i}—Zn2—O6	86.14 (4)	C24—C25—H25	119.9
O2—Zn2—O6	93.85 (4)	C35—C34—N3	120.97 (15)
O2—Zn2—O4	96.22 (4)	C39—C34—N3	119.10 (16)
O2^{i}—Zn2—O4	83.78 (4)	C39—C34—C35	119.92 (16)
O2^{i}—Zn2—O4^{i}	96.22 (4)	O3—C14—C15	118.44 (12)
O2—Zn2—O4^{i}	83.78 (4)	O4—C14—O3	119.60 (13)
O2^{i}—Zn2—O2	180.0	O4—C14—C15	121.96 (12)
C14—O3—Zn1	104.17 (9)	C30—C31—H31	119.7
C27—O5—Zn1	127.60 (9)	C32—C31—C30	120.62 (14)
C27—O6—Zn2	137.10 (9)	C32—C31—H31	119.7
C14—O4—Zn2	161.37 (10)	C3—C4—H4	119.5
Zn1—O7—H7A	129.0 (18)	C5—C4—C3	121.07 (14)
Zn1—O7—H7B	123.9 (19)	C5—C4—H4	119.5
H7A—O7—H7B	106 (3)	O5—C27—C28	115.79 (12)
C1—O2—Zn2	142.24 (10)	O6—C27—O5	124.31 (13)
C1—O1—Zn1	123.40 (10)	O6—C27—C28	119.89 (12)
C16—N2—C21	125.40 (13)	C25—C24—H24	120.1
C16—N2—H2	118.8 (16)	C25—C24—C23	119.74 (15)
C21—N2—H2	115.4 (16)	C23—C24—H24	120.1

C33—N3—C34	122.70 (13)	O2—C1—O1	123.47 (14)
C33—N3—H3	114.7 (15)	O2—C1—C2	118.44 (14)
C34—N3—H3	118.4 (15)	O1—C1—C2	118.09 (13)
C3—N1—C8	125.41 (13)	C22—C23—C24	120.36 (16)
C3—N1—H1	118.4 (16)	C22—C23—H23	119.8
C8—N1—H1	115.7 (16)	C24—C23—H23	119.8
C28—C29—H29	118.9	C4—C5—H5	119.4
C30—C29—H29	118.9	C4—C5—C6	121.24 (15)
C30—C29—C28	122.13 (13)	C6—C5—H5	119.4
C29—C28—C33	119.06 (13)	C34—C35—H35	120.1
C29—C28—C27	118.00 (12)	C36—C35—C34	119.87 (19)
C33—C28—C27	122.94 (12)	C36—C35—H35	120.1
N2—C16—C17	120.21 (13)	C8—C9—H9	120.0
N2—C16—C15	121.75 (13)	C10—C9—H9	120.0
C17—C16—C15	117.98 (13)	C10—C9—C8	120.04 (17)
N3—C33—C28	122.43 (13)	C9—C8—N1	119.28 (15)
N3—C33—C32	119.45 (13)	C13—C8—N1	120.97 (15)
C28—C33—C32	118.03 (13)	C13—C8—C9	119.70 (15)
C3—C2—C1	123.36 (14)	C7—C6—C5	118.31 (15)
C7—C2—C3	119.75 (14)	C7—C6—H6	120.8
C7—C2—C1	116.86 (13)	C5—C6—H6	120.8
C21—C26—H26	120.0	C9—C10—H10	120.0
C25—C26—H26	120.0	C11—C10—C9	120.07 (17)
C25—C26—C21	120.06 (15)	C11—C10—H10	120.0
N1—C3—C2	121.58 (13)	C34—C39—H39	120.2
N1—C3—C4	120.70 (14)	C34—C39—C38	119.63 (19)
C4—C3—C2	117.71 (14)	C38—C39—H39	120.2
C26—C21—N2	118.72 (14)	C8—C13—H13	120.0
C22—C21—N2	121.48 (13)	C12—C13—C8	119.98 (17)
C22—C21—C26	119.69 (13)	C12—C13—H13	120.0
C29—C30—H30	120.7	C10—C11—H11	120.1
C29—C30—C31	118.65 (14)	C10—C11—C12	119.88 (16)
C31—C30—H30	120.7	C12—C11—H11	120.1
C33—C32—H32	119.3	C13—C12—C11	120.29 (18)
C31—C32—C33	121.37 (14)	C13—C12—H12	119.9
C31—C32—H32	119.3	C11—C12—H12	119.9
C2—C7—H7	119.1	C35—C36—H36	119.9
C6—C7—C2	121.88 (15)	C35—C36—C37	120.2 (2)
C6—C7—H7	119.1	C37—C36—H36	119.9
C16—C17—H17	119.5	C39—C38—H38	119.8
C18—C17—C16	121.07 (14)	C37—C38—C39	120.4 (2)
C18—C17—H17	119.5	C37—C38—H38	119.8
C21—C22—H22	120.0	C36—C37—H37	120.0
C23—C22—C21	119.94 (15)	C38—C37—C36	120.01 (18)
C23—C22—H22	120.0	C38—C37—H37	120.0

Zn1—O3—C14—O4	−0.51 (15)	C3—C4—C5—C6	−1.7 (3)
Zn1—O3—C14—C15	−179.36 (10)	C21—N2—C16—C17	18.7 (2)

Zn1—O5—C27—O6	1.2 (2)	C21—N2—C16—C15	−164.39 (14)
Zn1—O5—C27—C28	−178.84 (9)	C21—C26—C25—C24	−1.4 (2)
Zn1—O1—C1—O2	−2.4 (2)	C21—C22—C23—C24	−1.1 (3)
Zn1—O1—C1—C2	178.08 (10)	C30—C29—C28—C33	2.1 (2)
Zn2—O6—C27—O5	−34.5 (2)	C30—C29—C28—C27	−178.18 (14)
Zn2—O6—C27—C28	145.52 (11)	C7—C2—C3—N1	178.35 (16)
Zn2—O4—C14—O3	−71.0 (3)	C7—C2—C3—C4	−0.5 (2)
Zn2—O4—C14—C15	107.8 (3)	C7—C2—C1—O2	13.3 (2)
Zn2—O2—C1—O1	40.1 (3)	C7—C2—C1—O1	−167.15 (14)
Zn2—O2—C1—C2	−140.43 (14)	C17—C16—C15—C20	4.0 (2)
N2—C16—C17—C18	174.60 (15)	C17—C16—C15—C14	−172.21 (13)
N2—C16—C15—C20	−172.99 (14)	C19—C20—C15—C16	−3.0 (2)
N2—C16—C15—C14	10.8 (2)	C19—C20—C15—C14	173.35 (15)
N2—C21—C22—C23	176.60 (14)	C18—C19—C20—C15	0.4 (3)
N3—C33—C32—C31	179.89 (16)	C20—C19—C18—C17	1.3 (3)
N3—C34—C35—C36	179.26 (16)	C20—C15—C14—O3	−2.8 (2)
N3—C34—C39—C38	−179.35 (15)	C20—C15—C14—O4	178.34 (14)
N1—C3—C4—C5	−177.00 (16)	C15—C16—C17—C18	−2.4 (2)
N1—C8—C13—C12	−178.26 (16)	C25—C26—C21—N2	−175.45 (14)
C29—C28—C33—N3	179.21 (14)	C25—C26—C21—C22	0.7 (2)
C29—C28—C33—C32	−4.3 (2)	C25—C24—C23—C22	0.4 (3)
C29—C28—C27—O5	9.52 (19)	C34—N3—C33—C28	−157.76 (15)
C29—C28—C27—O6	−170.54 (13)	C34—N3—C33—C32	25.8 (2)
C29—C30—C31—C32	−2.4 (2)	C34—C35—C36—C37	0.0 (3)
C28—C29—C30—C31	1.3 (2)	C34—C39—C38—C37	0.2 (3)
C28—C33—C32—C31	3.3 (2)	C4—C5—C6—C7	0.2 (3)
C16—N2—C21—C26	−132.15 (16)	C27—C28—C33—N3	−0.5 (2)
C16—N2—C21—C22	51.8 (2)	C27—C28—C33—C32	175.99 (14)
C16—C17—C18—C19	−0.2 (3)	C1—C2—C3—N1	0.5 (2)
C16—C15—C14—O3	173.38 (13)	C1—C2—C3—C4	−178.34 (14)
C16—C15—C14—O4	−5.4 (2)	C1—C2—C7—C6	176.93 (16)
C33—N3—C34—C35	47.6 (2)	C35—C34—C39—C38	−0.1 (2)
C33—N3—C34—C39	−133.18 (17)	C35—C36—C37—C38	0.1 (3)
C33—C28—C27—O5	−170.79 (13)	C9—C8—C13—C12	−0.8 (3)
C33—C28—C27—O6	9.2 (2)	C9—C10—C11—C12	−1.4 (3)
C33—C32—C31—C30	0.0 (3)	C8—N1—C3—C2	178.42 (16)
C2—C3—C4—C5	1.9 (2)	C8—N1—C3—C4	−2.8 (3)
C2—C7—C6—C5	1.2 (3)	C8—C9—C10—C11	1.9 (2)
C26—C21—C22—C23	0.5 (2)	C8—C13—C12—C11	1.4 (3)
C26—C25—C24—C23	0.8 (3)	C10—C9—C8—N1	176.66 (15)
C3—N1—C8—C9	118.66 (18)	C10—C9—C8—C13	−0.8 (2)
C3—N1—C8—C13	−63.9 (2)	C10—C11—C12—C13	−0.3 (3)
C3—C2—C7—C6	−1.0 (3)	C39—C34—C35—C36	0.1 (2)
C3—C2—C1—O2	−168.80 (14)	C39—C38—C37—C36	−0.2 (3)
C3—C2—C1—O1	10.7 (2)		

Symmetry code: (i) −*x*+1, −*y*+1, −*z*+1.